EMF Waveform Optimization using the Permanent Magnet Volume-Integration Method

Maxime R. Dubois, *Member IEEE*, and João P. Trovão, *Member, IEEE*

***Abstract*— The emf expression can be derived with the PM volume-integration method, allowing easier optimization and prediction of the emf harmonic content. An analytical expression is developed for predicting the electromotive force (emf) waveforms and flux linkage resulting from the motion of permanent magnets (PM) in the case of two cylinders, where the outer cylinder carries a surface-mounted winding and the inner cylinder carries the PMs. The expressions are based on the PM Volume-Integration Method, which uses a volume integral calculated over the magnet volume, rather than the usual surface integral over the coil surface. The specific case of surface-mounted arc PM with radial magnetization is analyzed. An outer cylinder with infinitely thin winding distribution on its inner surface is considered. The chording factor, slot factor and spread factor are included in the analytical expression. The emf waveform and related harmonics are predicted analytically and validated by comparing with a finite element analysis and with experiment.**

***Index Terms*— Permanent magnet machines, analytical calculation, electromotive force, magnet width, harmonics, surface-mounted, radial magnetization, optimization and prediction of emf harmonics.**

I. Introduction

PERMANENT magnets (PM) mounted on the surface of a cylindrical rotor will create a varying magnetic flux when rotating coaxially with respect to an outer, fixed cylinder. A winding mounted on the inner surface of such outer cylinder will develop an electromotive force (emf) as prescribed by Faraday's law. Such a simple geometry is illustrated in fig. 1c). In this paper, attention is paid to the emf waveform created across such a winding upon the rotation of the inner rotor. The originality of the paper lies in the use of a novel method for deriving the emf waveform by expressing the magnetic flux created by the magnets in an alternate manner, which is obtained by a volume integral over the PM volume, rather than using the conventional surface integral over the stator coil. In past work [1], the authors have presented the PM Volume-Integration Method and how analytical expressions of the emf can be obtained in cases where magnet shapes are complex. In this paper, Radially-magnetized, surface-mounted permanent magnets are considered here. The authors believed there was a need for demonstrating the simplicity of the PM Volume-Integration Method in the case of a more conventional PM shape and magnetization pattern, by also including the winding distribution factors leading to simple emf analytical expressions. These allow easy harmonic optimization and both form the original contribution of the paper.

A classical 3-phase PM synchronous machine configuration is shown in fig. 1a), where 1 slot is managed per pole per phase (12 slots for 3 phases and 4 poles) and where every winding overlaps one entire pole pitch. Semi-closed slots are desirable,

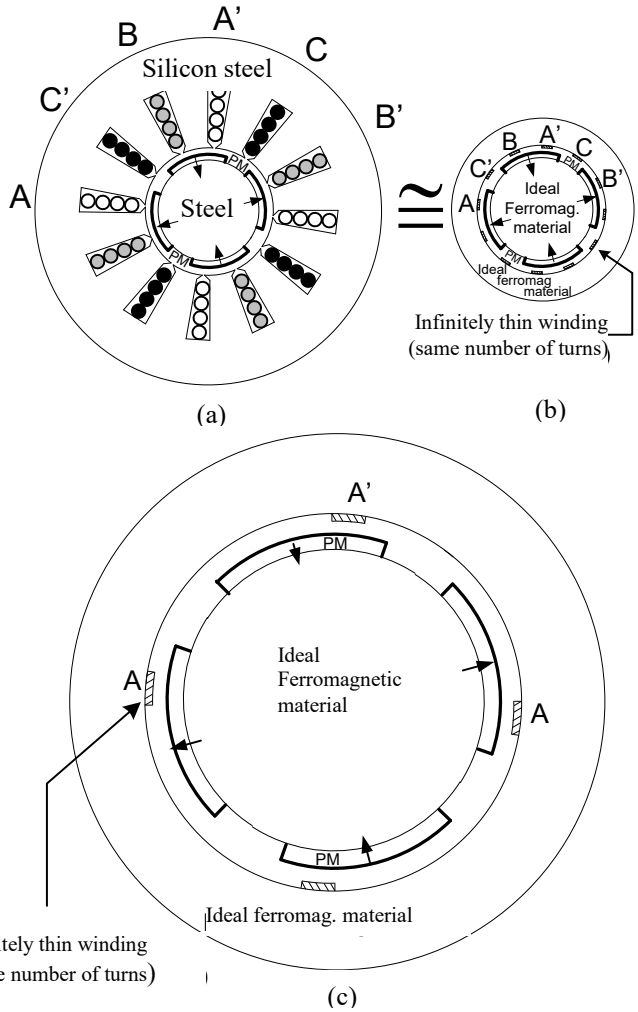

Fig. 1. (a) 3-phase PM synchronous machine with windings enclosed within semi-closed slots. (b) 3-phase PM machine with infinitely thin stator windings, equivalent for the emf. (c) Close-up view of the PM machine with infinitely thin stator winding. Only phase A is shown.

M. R. Dubois is with Université de Sherbrooke, Electrical and Computer Engineering Department, Sherbrooke, QC, CANADA (e-mail: maxime.dubois@usherbrooke.ca).

J. P. Trovão is with Université de Sherbrooke, Electrical and Computer Engineering Department, Sherbrooke, QC, CANADA (e-mail: joao.trovao@usherbrooke.ca).

in order to maximize the magnetic flux caught by the winding. The behavior of such a PM synchronous machine can be approached by that of the concentric cylinders of fig. 1b), where slots are removed and replaced by infinitely thin conductors disposed along the outer cylinder inner surface. Fig 1c) is identical to fig 1b), with the windings of phases B and C removed. Determining the harmonic content of the emf in the cylindrical configuration of fig. 1c) will find usefulness in industrial drive systems, as discussed in [2], even though the stator cylinder with infinitely thin winding does not account for the slot harmonics. Slot harmonics will certainly affect the torque ripple [3-6], but will not contribute to the machine useful torque. The two-cylinder approach with permanent magnets was also used in a number of papers [7-9].

As far as modifying the emf harmonics is concerned, increasing emf harmonics of ranks 3, 5, 7, 9 can be useful for generating trapezoidal emf waveform. Such trapezoidal emf can be used in combination with trapezoidal stator currents providing higher power density [10][11][4] in the machine and simpler drive control [12]. A well-known design approach to increase the emf harmonic content consists in setting the PM pole-arc ratio (ratio of PM width over pole pitch) close to 1.

In some other cases, emf harmonics 3, 5, 7, 9 are not desirable or have a detrimental effect [5]. It is then rather the fundamental component of the emf waveform that is looked for, in combination with sinusoidal phase currents. In this second design case, the emf waveform can be made almost sinusoidal and its harmonics strongly diminished by setting the PM pole-arc ratio in the range 0.5 to 0.7. Alternately, the emf harmonic content can also be altered by changing the coil distribution of the stator winding. For all these cases, there is a need for accurately predicting the harmonic content of the emf waveform.

A method often used to determine the emf waveform consists in computing the B and H fields of the magnetic circuit for different rotor positions, by using a 2-D finite-element software, then numerically calculate the integral of the B field over the winding area and finally derive the obtained value with respect to time [3][4][13][14]. This method can be applied to a set of designs until the emf waveform provides good results, which can be time consuming.

In [15], Sebastian *et al* have derived the fundamental component of the phase emf with the assumption of sinusoidally-distributed stator winding, using the assumption of 1-D straight magnetic paths for the PM flux density in the airgap. In [16], Almandoz *et al* have proposed an analytical procedure for expressing the emf waveform by expanding the PM remanent flux density B_r and the corresponding airgap field B_g into Fourier series. The stator winding distribution was also expanded into Fourier series and the emf harmonics was given as a product of field and winding distribution factor space harmonics. However, again, the field was assumed to follow 1-D straight paths in the airgap, which will not give an exact solution in the case of a thick air gap.

Great pieces of the electromagnetic theory were written on the analytical derivation of the airgap flux density field B, by solving Maxwell's equation in 2-D with proper boundary conditions. In particular, Zhu *et al* [8] and Boules *et al* [9] have derived analytical expressions in cylindrical coordinates, which formulate the 2-D radial and tangential components of the airgap flux density as a sum of harmonic components. Eventually, these expressions can be used to formulate the electromotive force e, by integrating the radial component of the airgap flux density B over a winding distribution of the stator expressed as a Fourier series, leading to an expression of the flux Ψ_0 linked by the stator winding. Taking motion into account and deriving Ψ_0 with respect to time would obviously lead to the emf. To our best knowledge, such mathematical paths have not been often followed. In these rare cases, only the procedure is expressed, as in [6][17][19]. Miller *et al* [19] have approached the problem of emf prediction by proposing exponential functions to model the north-south transitions (or fringing) between subsequent flux-density plateaus and by direct-construction of the emf waveform. Direct, accurate, 2-D analytical expressions of the emf waveform and related harmonics have been presented in 2014 by Wu *et al* [7] for surface-mounted PM machines. In the latter paper, the flux density function is obtained by solving the magnetic scalar potential function in the Laplace form in the airgap and in quasi-Poissonian form in the magnets. The outcome is a rather complex and lengthy mathematical approach, which can find limitations in the case of less conventional boundary conditions.

In the present paper, analytical expressions for the open-circuit flux linkage Ψ_0 and emf e seen by an infinitely thin stator winding located at the surface of the outer cylinder are developed in 2-D for a rotating inner cylinder with surface mounted, arc magnets with radial magnetization. The expressions are based on the theoretical work presented in [1][20] and present a method involving PM volume integration. Here, the emf will be determined by using a mathematical method different from [7] with a new resolution process and suiTABLE for optimization approach: the PM volume-integration method.

II. No-Load flux linkage with the PM-volume integration method: general considerations

A. Conventional expression of magnetic flux linkage and Faraday's law

From Faraday's law, the electromotive force e created across the winding terminals is expressed as the time derivative of the magnetic flux linkage Ψ_0 produced by the rotor magnets which links the coil. The magnetic flux linkage Ψ_0 is calculated by integrating the flux-density over the coil surface S of fig. 2, or mathematically:

$$\Psi_0 = \iint_S \vec{B}_0 \cdot d\vec{A}. \tag{1}$$

In (1), B_0 is the magnetic flux density crossing the coil surface in the space between the two cylinders and S is the coil surface, which may contain one or several turns. The field lines of B_0 are plotted in fig. 3, for the two-cylinder configuration, calculated from finite element analysis (FEA). B_0 is the flux density generated by the PMs, considering that no current

circulates in the stator windings. It is noTABLE that (1) implies that permanent magnets are a source of magnetic flux, the latter being collected by the coil. Hence, the coil flux linkage depends on the source of flux density (the PMs) and the collector geometry (the coil surface).

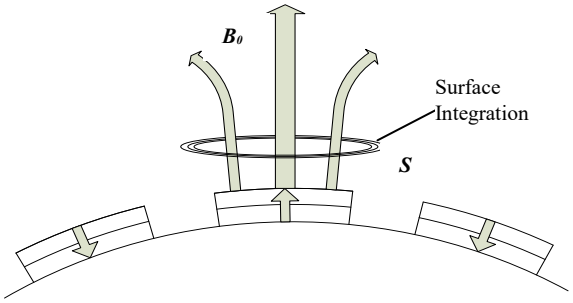

Fig. 2. Usual magnetic flux representation with the coil as a collector of B_0.

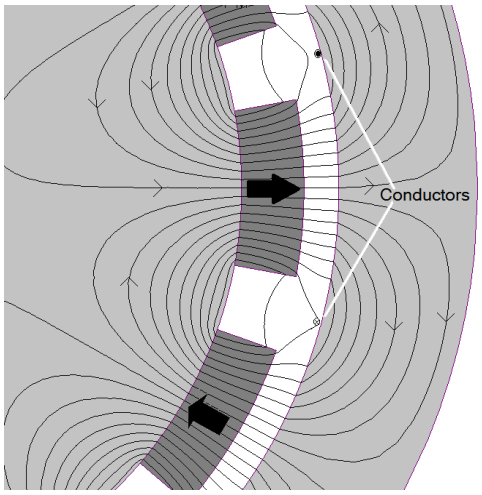

Fig. 3. Flux lines of B_0 created by the PM in a FEA of surface-mounted PM. Thin conductors are shown in the airgap.

B. Reciprocal relationship

A mathematical expression has been developed in [20] to express the flux linkage Ψ_0 in a different manner:

$$\psi_0 = \iiint_{V_{PM}} \frac{\vec{H}_a}{i} \cdot \vec{B}_r dV. \qquad (2)$$

In (2), H_a is the magnetic field intensity created by the stator coil alone (that is, when the PMs are replaced by air) upon the application of a current i in the coil. B_r is the PM remanent flux density and V_{PM} is the volume of the PMs. Here, we note that (2) is expressed as a volume integral, which is different from the conventional surface integration of (1). Equation (2) is mathematically equivalent to (1), as long as the following assumptions are met:

1) PMs have rigid magnetization, that is constant magnetization and recoil permeability $\mu_{recoil} = \mu_0$.
2) Steel parts are ideal (no saturation and infinite permeability).
3) Constant magnetic vector potential throughout the coil conductors cross-section, that is, assumption of filamentary conductors.

These 3 assumptions will be implicit throughout the paper. At this point, the reader may be uncomforTABLE with the idea that the flux linkage Ψ_0 expressed with (2) is equivalent to (1). However, the demonstration of this equivalence was well established in [20]. As a matter of fact, experimental results published in [1] have confirmed the validity of the PM-volume integration method. Moreover, the emf analytical expressions described in the rest of this paper and derived from (2) will also correlate with the emf obtained from both FEA and experiment as will be shown in section III.

The mathematical form of (2) suggests that the flux Ψ_0 linking the coil be viewed as a quantity obtained when a magnetic field H_a is produced by an infinitesimal current i flowing in that coil, the latter field H_a being collected by the PM volume elements. The calculation of H_a considers that all the PM volume elements are considered as empty space, as shown in fig. 4 and 5. Whence, (2) is reciprocal to the conventional expression for Ψ_0 where, in (2), the source of the magnetic interaction is the coil, whereas the collector geometry is the PM volume. This is shown in fig. 4 and 5.

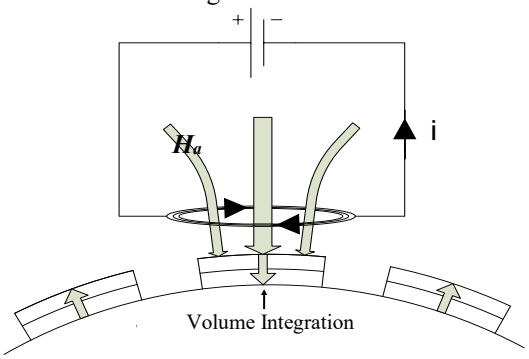

Fig. 4. Magnetic flux representation with PM volumes as a collector of H_a.

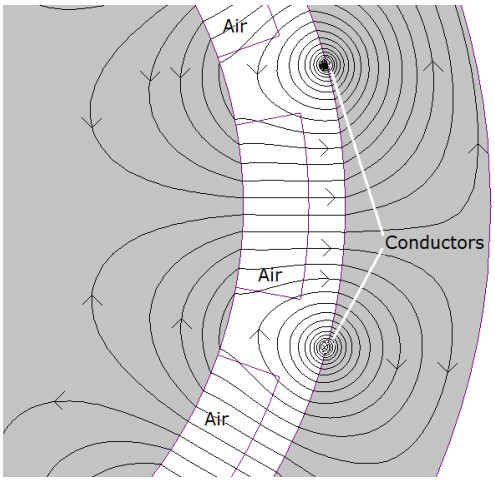

Fig. 5. Flux lines of H_a from 2-D FEA. H_a created by a current flowing in the conductors in a 2-cylinder configuration with PM volumes replaced by air.

In many cases, (2) will simplify the mathematical derivation of the emf and Ψ_0. Usually, determining B_0 implies solving Poisson's equation inside the magnets and Laplace equation in the airgap with the boundary conditions of the magnet elements of fig. 3, which can be a delicate task, when boundary conditions are more complex. On the other hand, solving H_a is

done by solving Laplace equation with circular boundaries, which is often much simpler. Also, the computation of magnetic flux with (1) requires the proper selection of the integration surface *S*, whereas the PM-volume integration implies that the volume elements are determined by the PM-volume geometry.

III. PM-VOLUME INTEGRATION METHOD: NO-LOAD FLUX LINKAGE AND EMF FOR CONCENTRIC CYLINDERS WITH SURFACE-MOUNTED PM

In this section, the PM volume-integration method described by (2) is used to derive an analytical expression of the electromotive force across the winding of Fig. 6. The PMs considered have a radial magnetization and are mounted on the surface of the rotor cylinder. In the cylindrical coordinate form, the dot product of (2) is transformed into

$$\Psi_0 = \int_0^{l_s}\int_{r_r}^{r_r+h_m}\int_{-\alpha_p/2}^{+\alpha_p/2}\left(\frac{H_{ar}}{i}B_{rr}+\frac{H_{a\alpha}}{i}B_{r\alpha}\right)r\,d\alpha\,dr\,dl, \quad (3)$$

where B_{rr} and $B_{r\alpha}$ are respectively the radial and tangential components of the PM remanent flux density. H_{ar} and $H_{a\alpha}$ are the radial and tangential components of the stator-created magnetic field in the airgap. Here, the flux linkage Ψ_0 is calculated for one stator coil with magnets replaced by air. The PM integral volume extends from radius $r = r_r$ to radius $r = r_r + h_m$, from mechanical angle $\alpha = -\alpha_p/2$ to $\alpha = +\alpha_p/2$, and from axial length $l = 0$ to $l = l_s$. As depicted in Fig. 6, r_r is the rotor radius, h_m is the thickness of the rotor magnets, l_s is the axial length of the stack of stator laminations and p is the number of pole pairs. Parameter α_p is the mechanical angle (in rad) occupied by one pole, which is equal to $\alpha_p = \pi/p$. With radially-magnetized PM, the tangential component $B_{r\alpha}$ is zero, leaving:

$$\Psi_0 = \int_0^{l_s}\int_{r_r}^{r_r+h_m}\int_{-\alpha_p/2}^{+\alpha_p/2}\left(\frac{H_{ar}}{i}B_{rr}\right)r\,d\alpha\,dr\,dl. \quad (4)$$

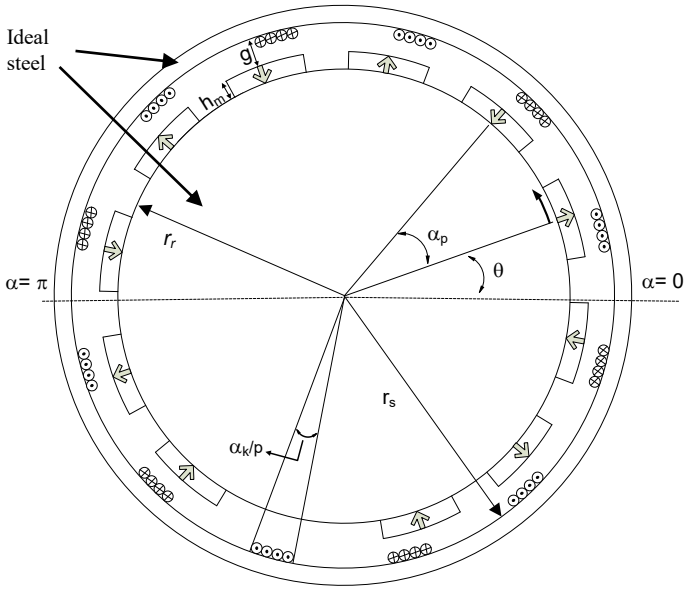

Fig. 6. Rotor and stator cylinders with their geometrical variables in a 12-pole configuration.

A. Magnetic field H_{ar} produced by the winding between the two cylinders

The stator-created field for the two-concentric cylinder problem with an infinitely thin winding was derived in previous scientific literature, by solving the magnetic vector potential expressed with Laplace equation [21]. The resulting H_{ar}/i gives

$$\frac{H_{ar}}{i}(\alpha) = \sum_{\kappa=1,3,5..}^{\infty}\frac{N_\kappa}{2r}\frac{(r^{2p\kappa}+r_r^{2p\kappa})}{(r_s^{2p\kappa}-r_r^{2p\kappa})}\left[\frac{r_s}{r}\right]^{p\kappa}\cos(p\kappa\alpha), \quad (5)$$

where H_{ar} is the radial component of the magnetic field intensity created in the space between the two cylinders, when magnets are replaced by air. α is the mechanical angle (see Fig. 6). κ is the rank of the harmonic considered. Equation (5) is expressed in terms of a sum of harmonic components and has only odd harmonics components due to the presence of a symmetrical winding. N_κ is the winding distribution factor, which accounts for how the thin coils are disposed along the inner surface of the cylinder. This coil distribution will have a significant effect on the emf waveform obtained across the winding. Section IV will pay special attention to the values of N_κ and the effect of the coil distribution.

B. Harmonic content of the magnetization for a surface-mounted arc PM

The radial component of the remanent flux density B_{rr} may also be expressed as a sum of harmonic components with respect to the circumferential angle α. For a rotor position of $\theta = 0$ rad, it can be viewed as the periodic function shown in fig. 7, which can be expressed as a Fourier series:

$$B_{rr}(\alpha)\big|_{\theta=0} = \sum_{\kappa=1,3,5...}^{\infty}B_{r\kappa}\cos(p\kappa\alpha), \quad (6)$$

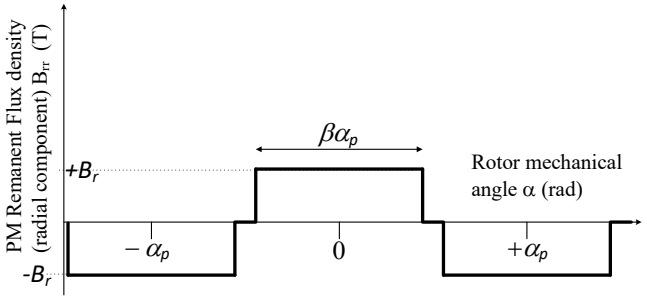

Fig. 7. PM remanent flux density distribution along the cylinder circumference for a standstill position ($\theta = 0$ degree).

where $B_{r\kappa}$ is the corresponding Fourier coefficients of the PM radial remanent flux density for each space harmonic. For a PM pole-arc ratio β, the amplitude of each harmonic will then be given by (7), that is,

$$B_{r\kappa} = \frac{4B_r}{\pi\kappa}\sin(\kappa\beta\frac{\pi}{2}). \quad (7)$$

B_r is the remanent flux density of the PM material and β is the PM pole-arc ratio. As the inner cylinder rotates with a given fixed velocity γ (in rpm), the rotor angular position θ increases at constant rate and B_{rr} can be written with,

$$B_{rr}(\alpha,\theta)=\sum_{\kappa=1,3,5...}^{\infty}B_{r\kappa}\cos(p\kappa\alpha)\cos(\kappa\theta) \tag{8}$$

C. Analytical expressions for the open-circuit flux linkage and emf

The volume integral over the PM boundaries is obtained by inserting (5)-(8) into (4) (detailed in [1]):

$$\Psi_0(\theta)=\frac{\pi l_s r_r}{4p}\sum_{\kappa=1,3,5...}^{\infty}\frac{B_{r\kappa}N_\kappa}{\left[1-\left(\frac{r_r}{r_s}\right)^{p\kappa}\right]\left[1+\left(\frac{r_s}{r_r}\right)^{p\kappa}\right]} \cdot\left[\frac{\left(1+\frac{h_m}{r_r}\right)^{1+p\kappa}-1}{1+p\kappa}+\frac{\left(1+\frac{h_m}{r_r}\right)^{1-p\kappa}-1}{1-p\kappa}\right]\cos(\kappa\theta). \tag{9}$$

The mathematical formulation of (9) considers an equal number of stator and rotor poles. As can be expected from a symmetrical stator and rotor, only odd harmonics are obtained. The emf $e(\theta)$ is obtained by deriving (9) with respect to time, θ being the only term varying with time. Here, it is the emf across the entire winding that is looked for, when all coils are connected in series. The result obtained should then be multiplied by the number of poles $2p$, giving eq. (10). In (9), Ψ_0 is the flux linkage caught by one stator pole and its winding, whereas in (10), e is the total stator emf with all stator windings connected in series.

$$e\ (\theta)=-\frac{\pi^2 l_s r_r p\gamma}{60}\sum_{\kappa=1,3,5...}^{\infty}\frac{B_{r\kappa}N_\kappa\kappa}{\left[1-\left(\frac{r_r}{r_s}\right)^{p\kappa}\right]\left[1+\left(\frac{r_s}{r_r}\right)^{p\kappa}\right]} \cdot\left[\frac{\left(1+\frac{h_m}{r_r}\right)^{1+p\kappa}-1}{1+p\kappa}+\frac{\left(1+\frac{h_m}{r_r}\right)^{1-p\kappa}-1}{1-p\kappa}\right]\sin(\kappa\theta). \tag{10}$$

Eq. (9)-(10) exhibit a dependence on the PM remanent flux density and corresponding space harmonics $B_{r\kappa}$. The distribution of the winding, given by N_κ, on the surface of the outer cylinder will also impact the waveform and harmonics of $\Psi_0(\theta)$ and $e(\theta)$. Eq. (10) highlights one essential condition for which any harmonic can be found in the emf spectrum: the harmonic component must be found in both the PM space harmonics $B_{r\kappa}$ and stator winding space distribution N_κ.

IV. Winding configuration and N_κ

N_κ is the winding distribution factor for each harmonic [21]. The distribution of the stator conductors along the stator core inner circumference is modeled by the number of conductors $n(\alpha)$ as a function of the mechanical angle α. The value N_κ considered in (5) assumes that $n(\alpha)$ is expressed by a Fourier series as [21]:

$$n(\alpha)=\sum_{\kappa=1,3,5...}^{\infty}\frac{1}{2}N_\kappa\sin(p\kappa\alpha), \tag{11}$$

where

$$N_\kappa=\frac{4N}{\pi}\sin\left[\frac{\pi\kappa}{2}\right]\cdot k_{d\kappa}k_{c\kappa}k_{s\kappa}, \tag{12}$$

and where N is the total number of turns in the machine and κ is the order of the harmonic [21]. The scientific literature has abundantly discussed how the various winding configurations affect the values of N_κ. Factors $k_{d\kappa}$, $k_{c\kappa}$, $k_{s\kappa}$ are respectively, the winding spread factor, chording factor and slot factor. The definition of these 3 factors is classical (given in Appendix).

The emf is obtained as a function of the winding factors by inserting (7) and (12) into (10):

$$e(\theta)=-\frac{4l_s r_r p\gamma N B_r}{15}\sum_{\kappa=1,3,5...}^{\infty}\frac{\sin\left[\frac{\pi\kappa}{2}\right]\sin(\kappa\beta\frac{\pi}{2})}{\left[1-\left(\frac{r_r}{r_s}\right)^{p\kappa}\right]\left[1+\left(\frac{r_s}{r_r}\right)^{p\kappa}\right]}k_{d\kappa}k_{c\kappa}k_{s\kappa} \cdot\left[\frac{\left(1+\frac{h_m}{r_r}\right)^{1+p\kappa}-1}{1+p\kappa}+\frac{\left(1+\frac{h_m}{r_r}\right)^{1-p\kappa}-1}{1-p\kappa}\right]\sin(\kappa\theta). \tag{13}$$

Eq. (13) is the analytical expression of the electromotive force that was looked for, which accounts for any winding configuration.

V. Validation of the EMF expression

The electromotive force waveform and its harmonic components can be predicted with (13). The relative weight of the harmonics will depend on the number of pole pairs p, PM pole-arc ratio β, magnet thickness h_m, stator and rotor radii r_s and r_r and the three winding factors $k_{d\kappa}$, $k_{c\kappa}$, $k_{s\kappa}$.

To determine the validity of (13), the emf waveform will first be calculated analytically with (13) and compared with the Finite Element Method in one given machine configuration, for 2 given values of β. Then, in section V.B, a comparison of the emf waveform calculated analytically with (13) will be made with experimental results.

A. Validation for a full-pitch winding: Analytical vs Finite Element Method

For a full-pitch winding like the one shown in Fig. 6, we have $k_{d\kappa}=k_{c\kappa}=1$ for all harmonics. The expression for $k_{s\kappa}$ detailed in appendix I is inserted in (13), yielding:

$$e(\theta) = -\frac{4 l_s r_r p \gamma N B_r}{15} \sum_{\kappa=1,3,5...}^{\infty} \frac{\sin\left[\frac{\pi\kappa}{2}\right] \sin(\kappa\beta\frac{\pi}{2}) \sin\left[\frac{\alpha_k \kappa}{2}\right]}{\left[1-\left(\frac{r_r}{r_s}\right)^{p\kappa}\right]\left[1+\left(\frac{r_s}{r_r}\right)^{p\kappa}\right]\left[\frac{\alpha_k \kappa}{2}\right]} \cdot \left[\frac{\left(1+\frac{h_m}{r_r}\right)^{1+p\kappa}-1}{1+p\kappa} + \frac{\left(1+\frac{h_m}{r_r}\right)^{1-p\kappa}-1}{1-p\kappa}\right] \sin(\kappa\theta). \quad (14)$$

Eq. (14) is the central element of the paper. It allows expressing the emf as a function of time and optimizing its harmonic content, as will be described further in the paper. To validate (14) with the specifications listed in TABLE I was investigated. The emf expression described by (14) was calculated as a function of the electrical angle θ for 5 values of the PM pole-arc ratio β. The resulting waveforms are presented in Fig. 8.

TABLE I
GEOMETRY OF THE PMSM USED IN THE FEM AND EXPERIMENT

Parameters	Symbol		Units
Number of poles	$2p$	12	—
Number of turns	N	5	—
Rotor radius	r_r	0.061	m
Stator radius	r_s	0.075	m
Airgap thickness	g	5	mm
Magnet thickness	h_m	9	mm
Coil width (electrical angle)	α_k	2.3	°
Magnet remanent flux density	B_r	1.15	T
Coil length	l_s	20	mm
Rotational speed	γ	1462	rpm

TABLE II presents the amplitude of the emf harmonic components of rank 1 to 7, calculated with (14) with the geometry detailed in TABLE I. From fig. 8 and TABLE II, it is noted that a PM pole-arc value of $\beta = 0.6$ will provide a more sinusoidal emf, whereas a β value higher than $\beta = 0.8$ will provide a more squary waveform. Fig. 8 also shows a dashed waveform, corresponding to a PM pole-arc ratio of $\beta = 0.405$, which will be the value used in the experimental machine presented in section III.B.

The same geometry (TABLE I) was implemented in Infolytica Magnet VII Finite Element Package. A 2-D magnetostatic simulation was carried out for 44 increasing electrical angles of the inner cylinder between 0 and 180 degrees electrical. For each electrical angle value, the flux linking the stator winding was computed and the electromotive force could be estimated from the flux variation between two successive angles.

As finite element method (FEM) implies some computational inaccuracy when computing the flux linkage, great care was taken in the simulation. Automatic meshing adaption was enabled, until a 0.01% difference in magnetostatic energy could be reached between two subsequent meshing patterns. Fig. 9 illustrates the flux line distribution after FEM field computation obtained for $\beta = 0.2$. Fig. 10 shows the results of the emf computed with the aid of the FEA package. The emf difference between (14) and the FEA is plotted on the graph of Fig. 11. The average difference is 0 V and the most significant difference observed at one point is 40 mV.

TABLE II
AMPLITUDE OF EMF HARMONIC COMPONENTS FROM (14)

Pole-arc ratio β	$\kappa = 1$	$\kappa = 3$	$\kappa = 5$	$\kappa = 7$	Units
1.0	1.67	0.28	0.07	0.02	V
0.8	1.59	0.16	0.00	0.01	V
0.6	1.36	0.09	0.07	0.01	V
0.405	1.02	0.27	0.00	0.02	V
0.2	0.52	0.23	0.07	0.02	V

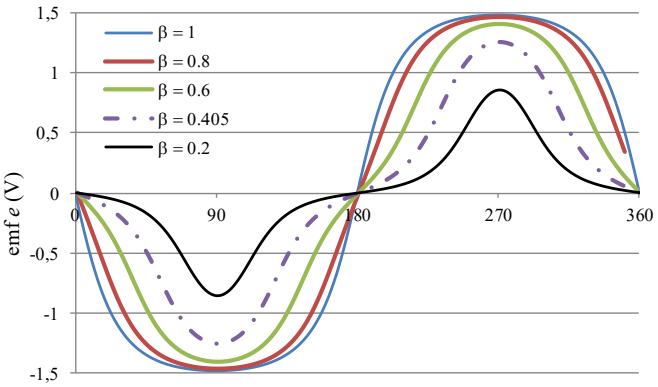

Fig. 8. Theoretical waveform obtained in 2-D with (14) for the geometry of TABLE I and PM pole-arc ratios of $\beta = 0.2, 0.405, 0.6, 0.8, 1$. The waveform for $\beta = 0.405$ is shown with a dash line, as it also represents the condition of the experimental set-up presented in the next section.

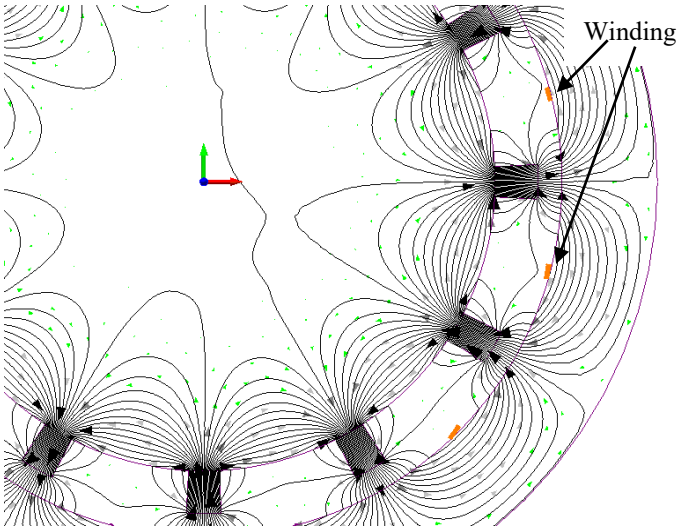

Fig. 9. Finite element model of the PMSM with PM pole-arc ratio $\beta = 0.2$ in rotor position $\theta = 0$.

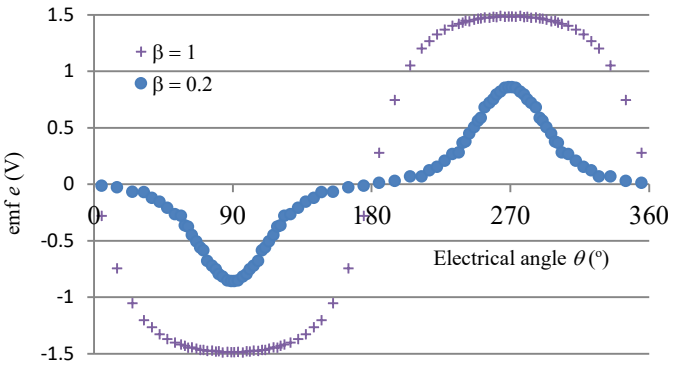

Fig. 10. Emf waveform obtained from 44 FEA Simulations. Geometry of TABLE I is considered and PM pole-arc ratios of $\beta = 0.2, 1$. Permanent Magnets $B_r = 1.15$ T and $\mu_{recoil} = \mu_0$.

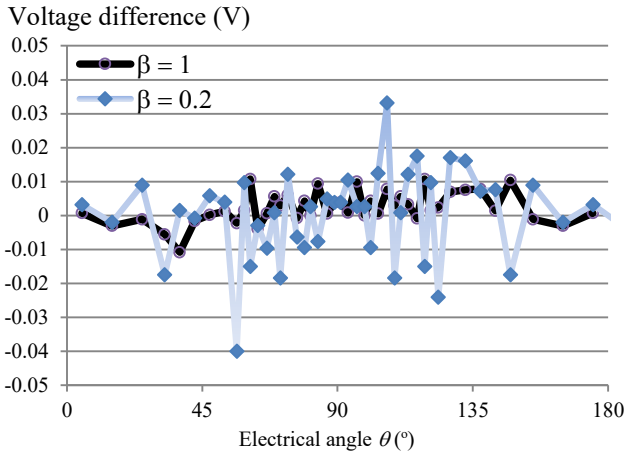

Fig. 11. Difference between (14) (fig. 8) and waveform from Finite Element Simulation (fig. 10). PM pole-arc ratios of $\beta = 0.2, 1$.

Most of the other points show a difference between theory and FEM of less than 10 mV. Due to the inherent property of Faraday's law, which implies computing the difference between two flux values at two successive instants, any small inaccuracy on each of the flux linkage FEM calculation will result in a higher error on the emf estimation. EMF computation using Finite Element simulation packages never provides perfect accuracy, even with the best precautions. All this being considered, it is reasonable to conclude that the analytical expressions of (14) is verified by the FEA.

B. Validation for a full-pitch winding: Analytical vs Experiment

An experiment was carried out with the rotor configuration of fig. 12 with the values listed in TABLE I inserted in the slotless stator of Fig. 13. In this experiment, the PM pole-arc ratio is set to $\beta = 0.405$. As illustrated in Fig. 13, only 1 pole of 5 turns was wound on the stator surface. The voltage was recorded across the winding at no-load. The measured waveform and the theoretical waveform predicted with (14) are shown in Fig. 14, with good agreement between theory and experiment.

A remark is made on the magnetization and shape of the magnets shown in Fig. 12. The rotor magnets were rectangular magnets instead of curved, arc magnets.

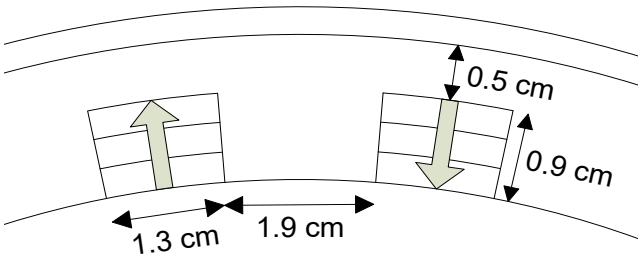

Fig. 12. Rotor geometry used in the experiment.

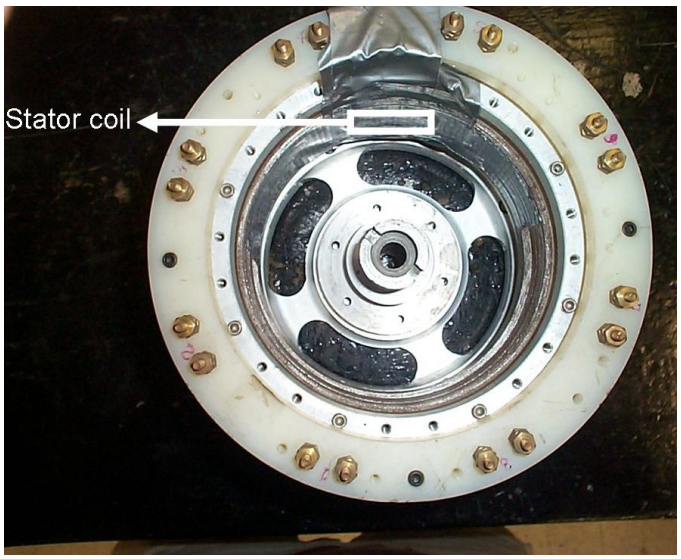

Fig. 13. Stator cylinder and position of the stator coil.

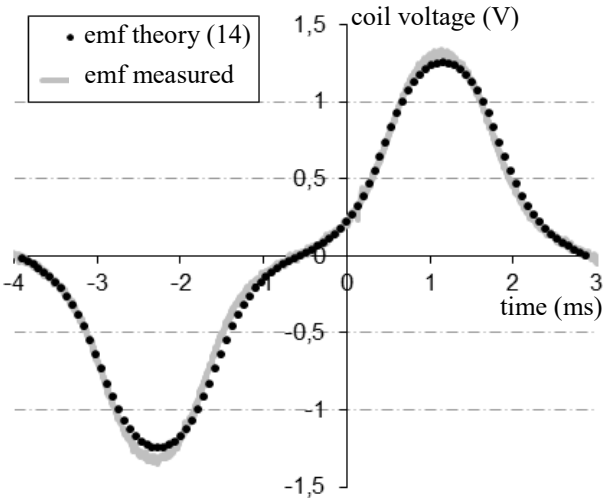

Fig. 14. Emf experimental waveform measured across the 5-turn stator coil and comparison with theoretical eq. (14). PM pole-arc ratio $\beta = 0.405$.

Also, the magnetization could not be made perfectly radial. These magnets were magnetized perpendicular to the magnet surface. These imperfections account for the small differences observed in Fig. 14 between theory and experiment.

VI. Optimization of Flux and Harmonic Content

Eq. (9) (no-load flux Ψ_0) and (14) (electromotive force e) can be used to optimize the PM pole-arc ratio β, in order to

investigate how β will influence the peak flux value and harmonics content.

The dimensions of the geometry described in TABLE I are inserted into (9), with airgaps value of $g = 2$ mm, 3 mm and 5 mm and identical magnet thickness. The resulting flux linkage Ψ_0 in the d-axis (for $\theta = 0$) is computed for increasing β values, with the corresponding results displayed in fig. 15. As can be expected, thinner airgaps will result in more flux linked by the stator coil. As the magnet width increases (increasing β), the flux Ψ_0 increases linearly up to a certain point. For $g = 2$ mm, with $\beta > 90\%$, the additional cost of PM material will create only a marginal flux increase. For $g = 5$ mm, this is also the case for $\beta > 80\%$. This difference is explained by the flux exchange between two adjacent magnets, which does not contribute to the flux seen by the stator conductor. With a thicker airgap, the amount of flux exchanged between neighboring magnets is higher than with thin airgaps.

For emf harmonic optimization, the derived expression (14) is used. Fig. 16 shows the ratio of the amplitudes of emf harmonics 3, 5, 7 over the amplitude of the fundamental, for two different airgap values. For trapezoidal emf waveform, a 2 mm-airgap with $\beta = 0.9$ will be best. For a sinusoidal waveform, $\beta = 0.7$ is a good compromise among harmonics 3, 5, 7. If harmonic 3 needs to be entirely suppressed, $\beta = 0.67$ will allow entire suppression of harmonic 3. This information will be useful especially when the stator windings are to be connected with a delta configuration.

From the results described in fig. 16, it is not possible to obtain entire suppression of all harmonics for a given β value. $\beta = 0.67$ will suppress harmonic 3, $\beta = 0.8$ will suppress harmonic 5 and $\beta = 0.86$ will suppress harmonic 7.

The resulting harmonic levels obtained with (14) and described in fig. 16 readily indicate that increasing the airgap thickness will reduce the harmonic content and thus enable more sinusoidal waveforms. Fig. 17 shows the emf waveforms predicted with thin ($g = 2$ mm) and thick ($g = 5$ mm) airgaps for a given magnet thickness ($h_m = 9$ mm) and stator bore diameter ($r_s = 7.5$ cm).

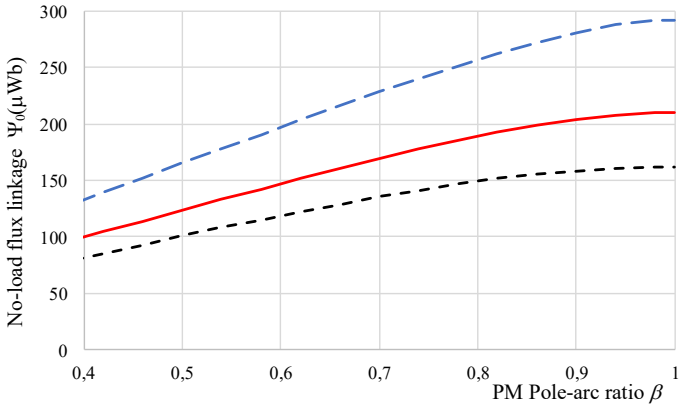

Fig. 15. Peak flux value obtained with equation (9) (all harmonics summed up) in the d-axis, as a function of the PM pole-arc ratio β. Geometry of TABLE I is inserted (9) with 3 airgap values ($g = 2$ mm, $g = 3$ mm, $g = 5$ mm). Magnet thickness $h_m = 9$ mm and stator bore diameter $r_s = 7.5$ cm for all three airgaps.

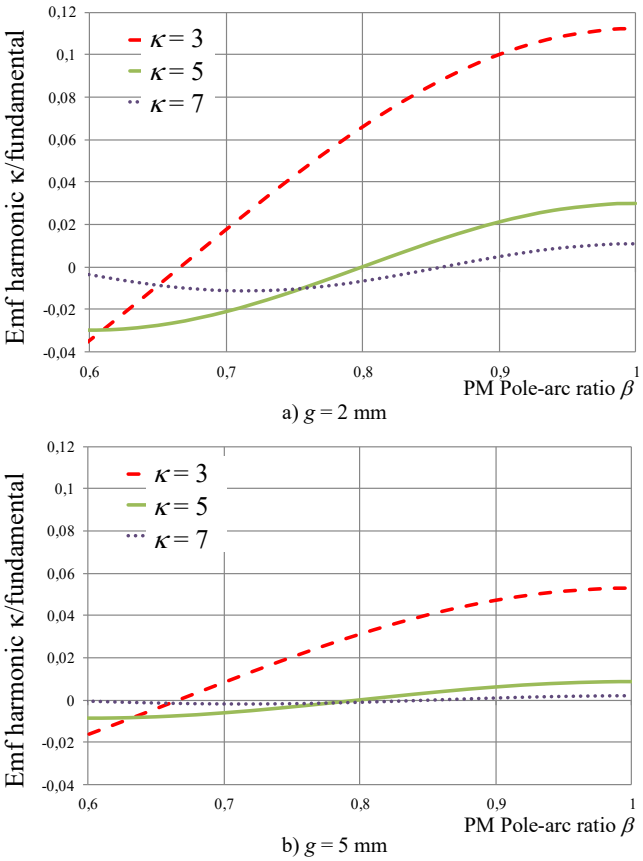

Fig. 16. Ratio emf harmonic κ over emf fundamental (harmonic 1), as a function of the PM pole-arc ratio β. These are theoretical results obtained with equation (14). Geometry of TABLE I is used with a) $g = 2$ mm b) $g = 5$ mm. Magnet thickness $h_m = 9$ mm and stator bore diameter $r_s = 7.5$ cm.

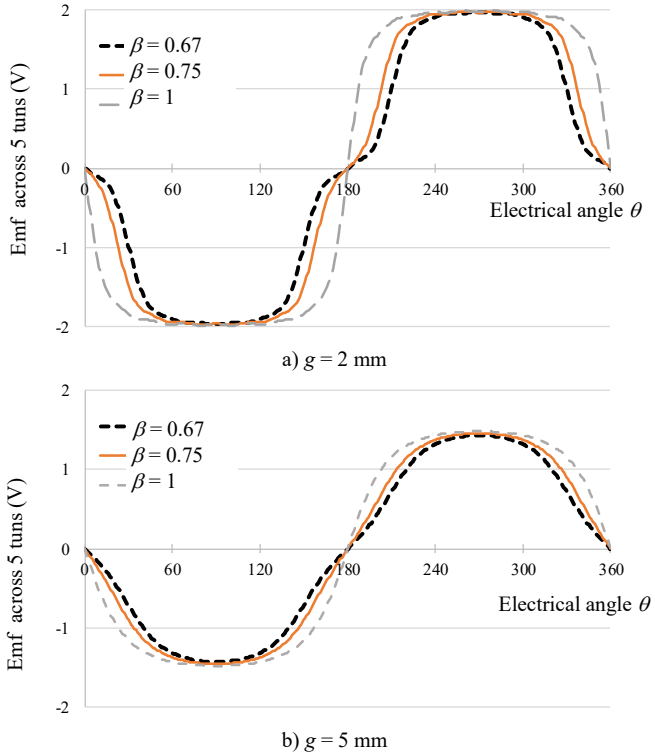

Fig. 17. Emf waveform $e(\theta)$ for $\beta = 0.67, 0.75, 1$. These are theoretical results obtained with equation (14). Geometry of TABLE I is used with a) $g = 2$ mm b) $g = 5$ mm. Magnet thickness $h_m = 9$ mm and stator bore diameter $r_s = 7.5$ cm.

VII. Conclusion

The paper has presented analytic expressions for the no-load flux linkage and the electromotive force of a PM synchronous machine with surface-mounted, arc magnets. These analytic expressions are derived from the previously developed concept of PM volumetric integration with the assumptions of rigid magnets and ideal, non-saturable stator and rotor cores. The methodology presented allows easy derivation of no-load flux whereas the 2-D circulation of the fields in the airgap is taken into account.

Equations (13) and (14) express the electromotive force e as a function of the rotor electrical angle θ, as a sum of harmonic components. The electromotive force calculated analytically with (14) is plotted for a given machine geometry with two PM pole-arc ratios of $\beta = 0.2$ and $\beta = 1.0$. These waveforms are compared to waveforms computed with FEM and show good agreement between analytical expressions calculated with the PM volume-integration method and FEA.

A comparison was also made between the emf waveform obtained from the analytical expression and from experimental data. Both waveforms correlate. These two validations (FEM and experimental), lead to conclude that the analytical expressions (9), (10), (13) for Ψ_0 and e are exact and usable for a winding mounted on the inner surface of an outer stator cylinder, and where the rotor is mounted with arc magnets with radial magnetization. These expressions will be useful for determining the emf in the case of a slotted stator with semi-closed slots. The case of PM with parallel magnetization is not studied in this paper (only radial magnetization here), but the PM volume integration method could be used in a similar manner in future works.

Finally, the flux linkage and emf expressions derived allow optimally selecting the PM pole-arc ratio β for harmonic maximization or minimization with various machine geometries, as was demonstrated in the last section of the paper.

Appendix: Winding Distribution Factors

The winding distribution is defined using 3 coefficients for each harmonic κ:

- Spread factor k_d: winding dispersion on multiple slots for each stator pole;
- Chording factor k_c: winding dispersion on the entire stator pole width (full-pitch) or a fraction of the stator pole width (short-pitch).
- Slotting factor k_s: winding dispersion due to the width of the slot opening;

Spread factor:

For one stator pole, the winding will occupy a given number of slots. The more slots are occupied by a winding, the more spread (or distributed) this winding will be

$$k_{d\kappa} = \frac{\sin\left[\frac{\kappa\pi}{2m}\right]}{q\sin\left[\frac{\kappa\pi}{2mq}\right]}, \tag{15}$$

where m is the number of phases and q is the number of slots per pole per phase. For $q = 1$, the winding is concentrated and for $q >> 1$, the winding will be very distributed.

Chording factor:

The winding can be configured to occupy a complete stator pole (full-pitch winding) or to occupy a width smaller than the pole pitch (short-pitch winding). Considering an integral number of stator slots, the winding will be short-pitched by discrete electrical angles. Short-pitching the stator winding will also affect the emf harmonics. The chording factor is defined as

$$k_{c\kappa} = \cos\left[\frac{\kappa\nu\pi}{2mq}\right], \tag{16}$$

ν is the number of slots by which the winding is short-pitched.

Slotting factor:

In a slotless, flat winding, the conductors will occupy a given width α_k. The slotting factor is defined as

$$k_{s\kappa} = \frac{\sin\left[\frac{\alpha_k\kappa}{2}\right]}{\left[\frac{\alpha_k\kappa}{2}\right]}, \tag{17}$$

where α_k is the slot opening in electrical radian. For wider values of α_k, the emf will be more sinusoidal and harmonics of higher ranks will be diminished.

References

[1] M. R. Dubois, G. Mailloux, "Analytical calculation of no-load voltage waveforms in machines based on permanent-magnet volume integration," *IEEE Trans. Magn.*, vol. 44, no. 5, pp. 581–589, May 2008.

[2] T. Sebastian and V. Gangla, "Analysis of induced EMF waveforms and torque ripple in a brushless permanent magnet machine," *IEEE Trans. Ind. Appl.*, vol. 32, no. 1, pp. 195-200, Sept. 1996.

[3] Z. Azar, Z.Q. Zhu, and G. Ombach, "Influence of Electric Loading and Magnetic Saturation on Cogging Torque, Back-EMF and Torque Ripple of PM Machines," *IEEE Trans. Magn*., vol. 48, no. 10, pp. 2650-2658, Oct. 2012.

[4] K. Wang, Z. Q. Zhu, and G. Ombach, "Torque Enhancement of Surface-Mounted Permanent Magnet Machine Using Third-Order Harmonic," *IEEE Trans. Magn.*, vol. 50, no. 3, March 2014.

[5] F. Wu, C. Tong, Y. Sui, L. Cheng and P. Zheng, "Influence of Third Harmonic Back EMF on Modeling and Remediation of Winding Short Circuit in a Multiphase PM Machine With FSCWs," *IEEE Trans. Ind. Electronics.*, vol. 63, no. 10, pp. 6031-6041, Oct. 2016.

[6] A. Rahideh, M. Mardaneh, and T. Korakianitis, "Analytical 2-D Calculations of Torque, Inductance, and Back-EMF for Brushless Slotless Machines With Surface Inset Magnets," *IEEE Trans. Magn.*, vol. 49, no. 8, pp. 4873-4884, Aug. 2013.

[7] L. Wu and Z.Q. Zhu, "Analytical Modeling of Surface-Mounted PM Machines Accounting for Magnet Shaping and Varied Property Distribution," *IEEE Trans. Magn.*, vol. 50, no. 7, July 2014.

[8] Z.Q. Zhu, D. Howe, and B. Ackermann, "Instantaneous magnetic field distribution in brushless permanent magnet dc motors, part I: open-circuit field," *IEEE Trans. Magn.*, vol. 29, no. 1, pp. 124-135, Jan. 1993.

[9] N. Boules, "Two-dimensional field analysis of cylindrical machines with permanent magnet excitation," *IEEE Trans. Ind. Appl.*, vol. IA-20, no. 5, pp. 1267-1277, Sept./Oct. 1984.

[10] K. Wang, Z. Q. Zhu, Y. Ren and G. Ombach, "Torque Improvement of Dual Three-Phase Permanent-Magnet Machine With Third-Harmonic Current Injection," *IEEE Trans. Ind. Electronics*, vol. 62, no. 11, pp. 6833-6844, Nov. 2015.

[11] K. Wang, Z. Y. Gu, Z. Q. Zhu, and Z. Z. Wu, "Optimum Injected Harmonics into Magnet Shape in Multi-Phase Surface-Mounted PM

Machine for Maximum Output Torque" *IEEE Trans. Ind. Electronics*, accepted for publication, Feb. 2017.

[12] T. Sebastian and V. Gangla, "Analysis of Induced EMF and Torque Waveforms in a Brushless Permanent Magnet Machine," *IEEE Trans. Ind. Appl.*, vol. 32, no. 1, pp. 195-200, Jan.-Feb. 1996.

[13] Joon-Ho Lee, Dong-Hun Kim, and Il-Han Park, "Minimization of Higher Back-EMF Harmonics in Permanent Magnet Motor Using Shape Design Sensitivity With B-Spline Parameterization," *IEEE Trans. Magn.*, vol. 39, no. 3, pp. 1269–1272, May 2003.

[14] A. Chen, R. Nilssen, and A. Nysveen, "Harmonic Analysis and comparison of the back EMFs of Four Permanent Magnet Machine with Different Winding Arrangements," in Int. Conf. Elec. Mach. and Syst., Wuhan, China, pp. 3043-3048, Oct. 2008.

[15] T. Sebastian, G. Slemon, and M.A. Rahman, "Modelling of Permanent Magnet Synchronous Motors," *IEEE Trans. Magn.*, vol. MAG-22, no. 5, pp. 1069-1071, Sept. 1986.

[16] G. Almandoz, J. Poza, M. A. Rodriguez, and A. Gonzalez, "Analytical Model of a PMSM Considering Spatial Harmonics," in Int. SPEEDAM Symp., Ischia, Italy, pp. 603-608, June 2008.

[17] P. Kumar and P. Bauer, "Improved Analytical Model of a Permanent-Magnet Brushless DC Motor," *IEEE Trans. Magn.*, vol. 44, no. 10, pp. 2299-2309, Oct. 2008.

[18] X. Wang, X. Zhang, S. Yan, X. Wang, and C. Zhang, "The analysis of high speed slotless permanent magnet brushless DC motor based on soft magnetic ferrite," in Int. Conf. Elec. Mach. and Syst, Tokyo, Japan, pp. 1061-1067, Oct. 2010.

[19] T.J.E. Miller and R. Rabinovici, "Back-EMF waveforms and core losses in brushless DC motors," *IEE Proc. Electr. Pow. Appl.*, vol. 141, Issue 3, pp. 144-154, May 1994.

[20] M. R. Dubois, H. Polinder, and J. A. Ferreira, "Contribution of permanent magnet volume elements to the no-load voltage in machines," *IEEE Trans. Magn.*, vol. 36, pp. 1784-1792, May 2003.

[21] H. Polinder, On the losses in a high-speed permanent-magnet generator with rectifier, Ph.D. dissertation, Delft Univ. Tech., Delft, The Netherlands, 1998.

Maxime R. Dubois (M'04) was born in Alma, QC, Canada. He received his PhD *cum laude* from Delft University of Technology (The Netherlands) in 2004. He received his B. Sc. in Electrical Engineering from the Université Laval, Québec, Canada in 1991.

Since 2004, he has been Faculty Member in two Canadian Universities. Between 2004 and 2011, he has been with the Université Laval (Quebec City). Since 2011, Prof. Dubois has been Associate Professor at the department of Electrical Engineering at Sherbrooke University, Canada. His fields of interest are electrical machines and power electronics applied to the field of wind energy, energy storage and electric vehicles. Dr. Dubois is a registered engineer, he is a member of the Institute of Electrical and Electronics Engineering and has published 75 papers in scientific journals and conference proceedings. He holds 6 international patents and acts as a consulting engineer on a regular basis. Professor Dubois was Technical Program Chair of the 2015 VPPC conference in Montréal, Canada. He is the founder of Eocycle Technologies Inc and founding professor of the companies AddEnergie Tech. and IngeniArts Tech.

João Pedro F. Trovão (S'08, M'13) was born in Coimbra, Portugal, in 1975. He received the MSc degree and the Ph.D. degree in Electrical Engineering from the University of Coimbra, Coimbra, Portugal, in 2004 and 2013, respectively. From 2000 to 2014, he was a Teaching Assistant and an Assistant Professor with the Polytechnic Institute of Coimbra–Coimbra Institute of Engineering (IPC–ISEC), Portugal. Since 2014, he has been a Professor with the Department of Electrical Engineering and Computer Engineering, University of Sherbrooke, Sherbrooke, QC, Canada, where he holds the Canadian Research Chair position in Efficient Electric Vehicles with Hybridized Energy Storage Systems. His research interests cover the areas of electric vehicles, hybridized energy storage systems, energy management and rotating electrical machines. J. P. F. Trovão was the General Co-Chair and the Technical Program Committee Co-Chair of the 2014 IEEE Vehicle Power and Propulsion Conference, as well as the Award Committee Member for the 2015 and 2016 IEEE Vehicle Power and Propulsion Conferences. He was a Guest Editor for the Special Issue of IET Electrical Systems in Transportation on Energy Storage and Electric Power Sub-Systems for Advanced Vehicles. He is a Guest Editor for the Special Issue of IEEE Transaction on Vehicular Technology on Electric Powertrains for Future Vehicles.